Eur Radiol (2016) 26:1871–1878
DOI 10.1007/s00330-015-3997-4

COMPUTED TOMOGRAPHY

Impact of an advanced image-based monoenergetic reconstruction algorithm on coronary stent visualization using third generation dual-source dual-energy CT: a phantom study

Stefanie Mangold[1,2] · Paola M. Cannaó[1,3] · U. Joseph Schoepf[1,4] · Julian L. Wichmann[1,5] · Christian Canstein[6] · Stephen R. Fuller[1] · Giuseppe Muscogiuri[1,7] · Akos Varga-Szemes[1] · Konstantin Nikolaou[2] · Carlo N. De Cecco[1,7]

Received: 25 February 2015 / Revised: 18 May 2015 / Accepted: 1 September 2015 / Published online: 15 September 2015

Abstract

Purpose To evaluate the impact of an advanced monoenergetic (ME) reconstruction algorithm on CT coronary stent imaging in a phantom model.

Materials and methods Three stents with lumen diameters of 2.25, 3.0 and 3.5 mm were examined with a third-generation dual-source dual-energy CT (DECT). Tube potential was set at 90/Sn150 kV for DE and 70, 90 or 120 kV for single-energy (SE) acquisitions and advanced modelled iterative reconstruction was used. Overall, 23 reconstructions were evaluated for each stent including three SE acquisitions and ten advanced and standard ME images with virtual photon energies from 40 to 130 keV, respectively. In-stent luminal diameter was measured and compared to nominal lumen diameter to determine stent lumen visibility. Contrast-to-noise ratio was calculated.

Results Advanced ME reconstructions substantially increased lumen visibility in comparison to SE for stents ≤3 mm. 130 keV images produced the best mean lumen visibility: 86 % for the 2.25 mm stent (82 % for standard ME and 64 % for SE) and 82 % for the 3.0 mm stent (77 % for standard ME and 69 % for SE). Mean DLP for SE 120 kV and DE acquisitions were 114.4±9.8 and 58.9±2.2 mGy×cm, respectively.

Conclusion DECT with advanced ME reconstructions improves the in-lumen visibility of small stents in comparison with standard ME and SE imaging.

Key Points

- *An advanced image-based monoenergetic reconstruction algorithm improves lumen visualization in stents ≤3.0 mm.*
- *Application of high keV reconstructions significantly improves in-stent lumen visualization.*
- *DECT acquisition resulted in 49 % radiation dose reduction compared with 120 kV SE.*

Keywords Dual-energy CT · Coronary CT · Stent · Monoenergetic imaging · Iterative reconstruction

Abbreviations

CCTA	Coronary computed tomography
DECT	Dual-energy computed tomography
keV	kilo-electron volts
ME	Monoenergetic
CNR	Contrast-to-noise ratio

✉ U. Joseph Schoepf
schoepf@musc.edu

1 Division of Cardiovascular Imaging, Department of Radiology and Radiological Science, Medical University of South Carolina, Ashley River Tower, 25 Courtenay Drive, Charleston, SC 29425-2260, USA

2 Department of Diagnostic and Interventional Radiology, Eberhard-Karls University Tuebingen, Tuebingen, Germany

3 Scuola di Specializzazione in Radiodiagnostica, University of Milan, Milan, Italy

4 Division of Cardiology, Department of Medicine, Medical University of South Carolina, Charleston, SC, USA

5 Department of Diagnostic and Interventional Radiology, University Hospital Frankfurt, Frankfurt, Germany

6 Siemens Medical Solutions, Malvern, PA, USA

7 Department of Radiological Sciences, Oncology and Pathology, University of Rome "Sapienza", Rome, Italy

SE	Single-energy
ECG	Electrocardiogram
$CTDI_{vol}$	Volume-based computed tomography dose index

Introduction

Non-invasive diagnostic workup of patients with coronary computed tomography (CCTA) after coronary artery stenting is still a challenging task, as blooming artefacts caused by beam hardening and partial volume effects impair stent visualization and result in underestimation of the stent lumen. While innovations in cardiac CT technology have led to high negative predictive values for exclusion of in-stent restenosis from 78 to 100 %, positive predictive values are markedly inferior, ranging between 18 and 89 % [1]. Thanks to technical improvements in image acquisition and post-processing, several new approaches to enhance the evaluation of coronary stent patency and in-stent stenosis have been developed. In particular, new iterative reconstruction algorithms and the use of high convolution kernels have recently shown promising results [2–8].

Another promising approach to improve image quality is dual-energy CT (DECT) acquisition, which enables the generation of virtual monochromatic images at different virtual kilo-electron volt (keV) levels [9–13]. Using single-source DECT, Stehli et al. were able to show that monoenergetic (ME) reconstructions from DECT acquisitions improve stent lumen visualization [14]. Recently, an advanced image-based ME algorithm (Dual Energy Monoenergetic Plus, Siemens, Forchheim, Germany) was introduced, which utilizes a frequency-based mixing of low keV images that provides a higher contrast signal and images from the keV level optimizing image noise. Thus, the images generated combine the benefits of both image stacks while overcoming the noise limitations associated with the standard ME technique (Dual Energy Monoenergetic, Siemens), allowing for significantly improved iodine contrast-to-noise ratios (CNR) in comparison to standard ME images and single-energy (SE) acquisitions [11–13].

The aim of this study was to comprehensively evaluate the impact of the advanced ME reconstruction algorithm on stent imaging in comparison to standard ME reconstructions and SE acquisition in a moving coronary stent phantom with third-generation dual-source DECT.

Materials and methods

Stents and phantom setup

Three commercially available drug-eluting stent systems, which are commonly used in clinical practice for percutaneous coronary intervention, were studied (Taxus Express^2 with inner diameters of 3.0 mm and 3.5 mm; Taxus Express^2 Atom with inner diameter of 2.25 mm; Boston Scientific Corporation, Natick, MA, USA). All stents were made of 316 L stainless steel with a strut wall thickness of 0.132 mm. Before being imaged, each stent was implanted on an identical polyurethane tube of a defined outer diameter (2.25, 3.0, and 3.5 mm), which served as a contrast-enhanced vessel specimen with an attenuation of 200 HU (CTIodine, QRM Quality Assurance in Radiology and Medicine GmbH, Moehrendorf, Germany). The artificial vessels were fixed in a specimen holder and positioned in a water-filled polymethyl methacrylate container held in place by a lever attached to a motion simulator (Motion Simulator Sim2D, QRM). The container was then placed in position of the heart in an anthropomorphic thoracic phantom resembling a human chest (Cardio CT Phantom, QRM). The movement of the lever was controlled by a computerized controller module, which simulated a bi-directional cardiac motion in the stent phantom, while generating a synchronous ECG signal (Fig. 1).

CT acquisition parameters

All examinations were performed with a third-generation dual-source DECT scanner (SOMATOM Force, Siemens) equipped with a fully integrated circuit detector system (Stellar Infinity, Siemens). Images were acquired with prospectively electrocardiogram (ECG)-triggered acquisition at 70 % of the RR interval using a simulated ECG from the cardiac motion phantom with a heart rate of 70 beats per minute and sinus rhythm. The scan parameters were as follows: detector collimation 2×64×0.6 mm for DE acquisition and 2×68×0.6 for SE acquisition, gantry rotation 0.25 s, 512×512 pixel matrix size, 190 mm reconstruction field of view. Tube potential was

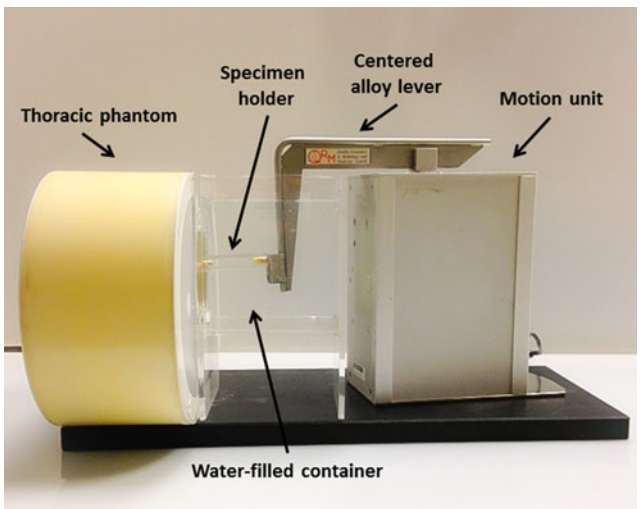

Fig. 1 Experimental set-up with a moving coronary stent phantom simulating a bi-directional cardiac motion while generating a synchronous ECG signal

set at a combination of 90 kV and 150 kV with tin filtration for DECT and 70, 90 and 120 kV for SE DSCT. Automated tube current modulation (CAREDose 4D, Siemens) was enabled for DE and SE and automated tube potential selection (CARE kV, Siemens) was set in "semi" mode in order to maintain constant iodine contrast to noise ratio (CNR) for the SE scans [15]. The volume-based computed tomography dose index ($CTDI_{vol}$) was automatically provided by the system and tube current and dose length product (DLP) were recorded for each acquisition.

Image reconstruction and analysis

All SE and DE images were reconstructed with a third-generation, advanced modelled iterative reconstruction algorithm (ADMIRE, Siemens) with strength 3 using a medium sharp convolution kernel (Bv49), 0.5 mm section thickness, and increment of 0.3 mm.

Using dedicated post-processing software (Syngo.via VA30 Dual Energy, Siemens) advanced and standard ME reconstructions were enabled with virtual photon energies of 40, 50, 60, 70, 80, 90, 100, 110, 120, and 130 keV. Overall, 23 image series were evaluated for each stent including three SE acquisitions and ten advanced and standard ME images, respectively, using the same post processing system. For each stent and image, reconstruction in-stent luminal diameter was measured manually on cross section images at three different levels using the electronic diameter calipers provided by the workstation's software. The reviewer was blinded to the applied image reconstruction and stent lumen diameter and a zoomed field of view with a fixed window level at 300 HU and window width of 1200 HU was used. Stent lumen visibility was calculated as the ratio of manual measurements of the stent lumen and nominal lumen diameter of the stent, given in percent.

For measurements of attenuation, circular regions of interest (ROI) were placed within the stent, carefully avoiding the stent components and blooming artefacts. ROIs were also placed in the carrier tube outside the stent as well as the water inside the phantom. Image noise was defined as the standard deviation (SD) of the attenuation in the surrounding water. Measurements were performed on three different sections of each stent and given as mean values. CNR was calculated as the difference of attenuation of in-stent iodine solution and attenuation of water divided by image noise.

Statistical analysis

Commercially available software (MedCalc Statistical Software, v12.7.5.0, MedCalc bvba, Belgium) was used for statistical analysis. For all numerical values derived from multiple measurements, the mean value and standard deviation (SD) were calculated. Lumen visibility and objective image quality parameters (noise and CNR) were plotted against tube potential. Dose reduction for low SE and DE tube potential acquisitions was calculated using the 120-kV acquisition on the same CT system as the reference standard.

Results

Measurement values for mean stent lumen, mean lumen visibility, attenuation of the carrier tube within sections inside and outside the stented area, image noise, and CNR are given in Table 1 for selected keV and kV levels. Objective image quality parameters (noise and CNR) plotted against tube potential for each stent are provided in Fig. 2 with representative CT images in Figs. 3, 4 and 5.

Attenuation, noise and CNR evaluation

In terms of objective image quality, advanced ME reconstructions provided increased CNR values in comparison to standard ME images and SE acquisitions (Table 1, Fig. 2). The highest CNR was found for the advanced ME reconstruction at 120 keV with a value of 8.1 for 2.25 mm, 6.5 for 3 mm, and 5.8 for 3.5 mm diameter stents. The maximum CNR for standard ME images was 3.9 at 70 keV and 5.6 at 120 keV with SE acquisition.

Lumen diameter evaluation

In advanced ME reconstructions, the in-stent diameters were substantially increased in comparison to standard SE images and slightly increased in comparison to the standard ME reconstruction algorithm for the 2.25 mm and 3.0 mm stent. The highest values for lumen visibility were found for 130 keV and advanced image based ME reconstructions with a lumen visibility of 82 % for the 3.0 mm stent (77 % for standard ME images and 69 % for SE acquisition) and of 86 % for 2.25 mm diameter stent (82 % for standard ME images and 64 % for SE acquisition). For 3.5 mm stents, the improvements in stent lumen visibility were less pronounced with mean values of 92 % for advanced ME images, 91 % for standard ME reconstructions and 87 % for SE acquisitions (Table 1, Fig. 2).

Radiation dose

SE image acquisition with a tube voltage of 120 kV, 90 kV, and 70 kV resulted in a mean $CTDI_{vol}$ of 12.0±2.4, 5.6±0.7 and 3.8±1.0 mGy as well as a DLP of 114.4±9.8, 59.7±6.1, and 36.5±1.9 mGy×cm, respectively.

The DE acquisition resulted in a mean $CTDI_{vol}$ of 5.5±0.7 mGy and a DLP of 58.9±2.2 mGy×cm, which represents a 49 % reduction in comparison with the standard 120 kV SE acquisition (Fig. 6).

Table 1 Mean stent lumen, mean lumen visibility), attenuation values of the tube inside and outside the stented area as well as noise values and contrast-to-noise ratio (CNR) for selected kiloelectron (keV) and kilovolt levels (kV)

	40 keV Mono+	70 keV Mono+	90 keV Mono+	120 keV Mono+	130 keV Mono+	40 keV Mono	70 keV Mono	90 keV Mono	120 keV Mono	130 keV Mono	70 kV Standard	90 kV Standard	120 kV Standard
2.25 mm													
Stent lumen (mm)	1.3±0.2	1.6±0.2	1.7±0.1	1.9±0.1	1.9±0.2	1.2±0.2	1.5±0.2	1.7±0.1	1.8±0.1	1.8±0.1	1.3±0.1	1.5±0.2	1.4±0.1
Mean lumen visibility (%)	57.8	69.6	77.0	84.4	85.9	54.8	68.1	74.1	80.0	81.5	59.3	65.2	63.7
In-stent attenuation (HU)	400.1±61.5	223.9±25.5	204.5±19.4	191.6±28.0	189.7±29.1	383.6±97.1	226.8±8.4	195.1±22.1	175.6±33.6	172.2±35.7	246.0±78.1	318.0±39.0	226.7±60.2
Tube attenuation outside stented area (HU)	274.2±66.8	151.1±31.8	126.1±24.7	109.7±17.2	107.2±16.1	237.6±119.5	148.3±22.7	130.2±4.8	119.0±10.2	117.2±12.0	200.0±9.5	231±6.1	172.7±20.6
Noise (HU)	75.0±2.9	32.9±1.3	26±1.1	23.2±0.8	24.1±1.0	245.6±3.6	47.4±0.9	52.8±1.7	72.0±2.4	75.9±2.5	62.0±3.0	62.7±1.2	40.7±5.8
CNR	5.4	6.7	7.8	8.1	7.4	1.6	4.8	3.6	2.4	2.2	3.9	5.1	5.6
3.00 mm													
Stent lumen (mm)	1.9±0.1	2.2±0.1	2.3±0.1	2.4±0.1	2.5±0.1	2.0±0.1	2.1±0.2	2.2±0.1	2.3±0.1	2.3±0.1	2.0±0.2	2.1±0.1	2.1±0.1
Mean lumen visibility (%)	64.4	74.4	76.7	81.1	82.2	65.6	71.1	74.4	75.6	76.7	65.6	68.9	68.9
In-stent attenuation (HU)	326.5±261.9	222.2±74.9	209.7±37.0	207.5±29.6	206.5±31.4	221.5±122.1	198.6±35.8	214.2±22.2	223.8±18.3	225.4±18.3	317.7±88.6	229.3±30.4	225.7±46.9
Tube attenuation outside stented area (HU)	350.1±18.6	193.6±16.7	161.1±11.0	140.1±6.2	136.5±5.5	312.3±27.0	176.7±9.7	149.3±6.6	132.5±5.1	129.5±4.9	189.7±5.6	205.3±9.1	197.7±27.1
Noise (HU)	105.9±7.1	45.5±2.4	35.8±2.1	31.8±2.4	32.3±2.7	245.6±8.2	47.4±1.8	52.8±2.2	72.0±2.9	75.9±3.0	100±2.0	58.7±2.9	42.3±1.5
CNR	3.1	4.9	5.8	6.5	6.4	0.9	4.2	4.0	3.1	2.9	3.2	3.9	5.3
3.5 mm													
Stent lumen (mm)	2.7±0.1	3.1±0.1	3.0±0.2	3.2±0.1	3.2±0.1	2.8±0.1	3.0±0.1	3.1±0.1	3.1±0.1	3.2±0.1	2.9±0.1	3.0±0.2	3.0±0.1
Mean lumen visibility (%)	76.2	88.6	86.7	91.4	92.4	79.1	84.8	88.6	89.5	90.5	83.8	84.8	86.7
In-stent attenuation (HU)	292.1±100.8	225.3±12.1	198.5±9.5	191.8±17.9	190.6±19.4	376.7±125.2	234.0±11.2	205.2±20.9	187.5±34.8	184.4±37.2	242.7±10.5	210.7±23.1	215.7±11.4
Tube Attenuation outside stented area (HU)	316.6±82.6	204.4±20.1	162.4±17.7	145.6±15.7	143.6±14.5	262.9±84.5	186.0±4.9	170.5±21.4	161.0±32.2	159.3±34.0	211.0±25.7	212.3±13.6	160.3±6.0
Noise (HU)	110.5±12.1	47.7±4.0	37.7±2.7	33±2.0	33±1.9	245.6±22.3	47. ± 4.5	52.6±3.5	71.0±4.9	75.3±5.1	75.7±2.3	60±4.4	41.7±3.1
CNR	2.8	4.7	5.3	5.8	5.7	1.6	4.9	3.8	2.6	2.4	2.8	3.5	5.2

Mono+: Advanced monoenergetic algorithm, Mono: standard monoenergetic algorithm, HU: Hounsfield units, mean value±standard deviation

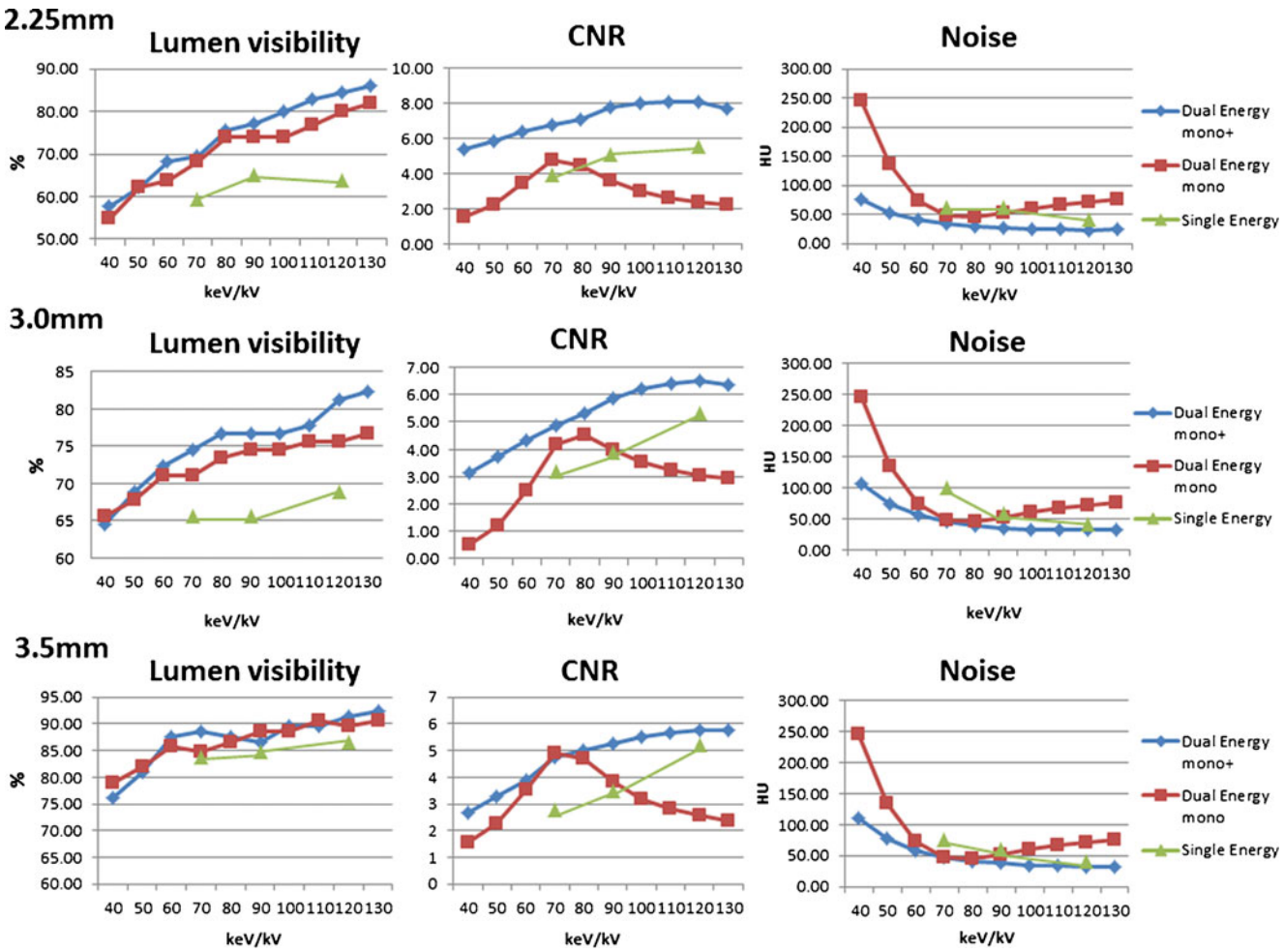

Fig. 2 Lumen visibility, noise and contrast-to-noise ratio (CNR) plotted against tube potential for each stent diameter show substantially increased in-stent diameter in advanced and standard monoenergetic images (mono+ and mono) in comparison to single-energy images for 2.25 mm and 3.0 mm diameter stents as well as higher CNR and slightly lower noise levels in mono+ images. For the 3.5 mm diameter stent the improvements in stent lumen visibility were less pronounced

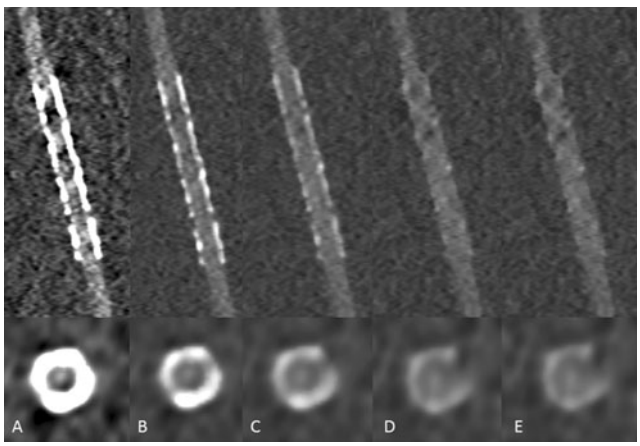

Fig. 3 Image-based advanced monoenergetic images with virtual photon energies of 40 keV (A), 70 keV (B), 90 keV (C), 120 keV (D), and 130 keV (E) of the 3.0 mm stent phantom in multiplanar reformats and cross section images show better lumen visualization and reduced blooming artefacts of the stent with increasing keV levels. The same window settings are used in A–E (bone window setting; centre/width 300/1200 HU)

Discussion

By combining the use of a third-generation dual-source DECT system equipped with a fully integrated circuit detector system and an advanced ME reconstruction algorithm, we were able to demonstrate improved in-stent lumen visualization in comparison with standard ME and SE data-sets in stents with a diameter of 2.25 and 3.0 mm.

Improvements in stent lumen visibility were less pronounced for the 3.5 mm stent, which correlates with previous studies describing how the effects of imaging refinements become marginal for stents larger than 3 mm [16]. Stents with a diameter <3 mm are more likely to be too small to evaluate [17–19] and guidelines generally do not recommend the use of CCTA for their assessment [20]. The applications of our initial findings to clinical practice could therefore expand the indications for CCTA to include small stent assessment.

In addition, the advanced ME reconstruction algorithm allows for significant improvement in iodine CNR in

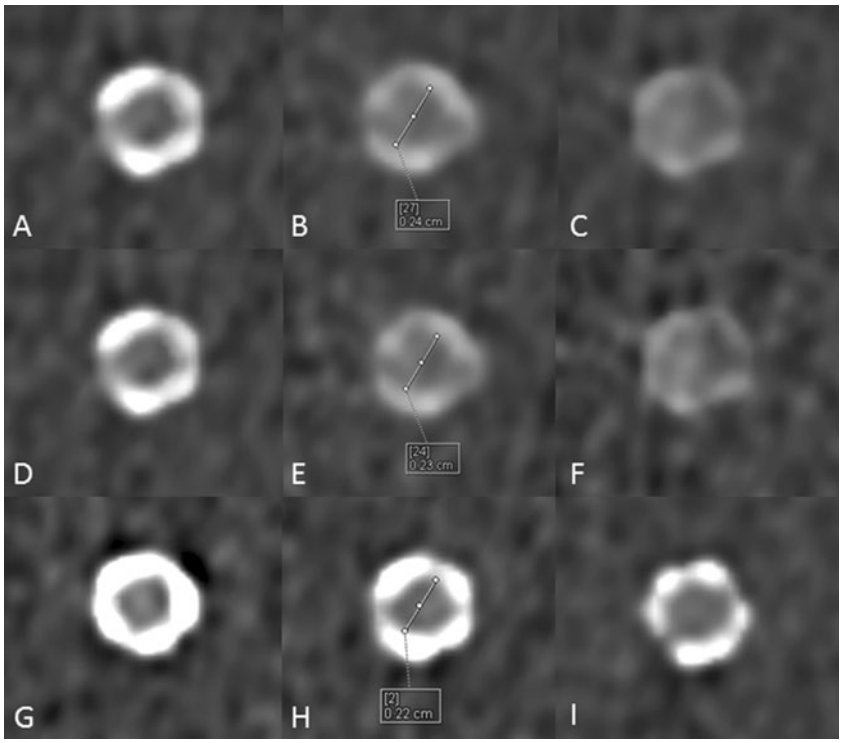

Fig. 4 Cross section images of advanced (A-C) and standard (D-F) monoenergetic images at 70, 90, and 120 keV, respectively, as well as single-energy images at 70, 90, and 120 kV (G-I) of the 3.0 mm stent. The monoenergetic images result in a better lumen visualization in comparison to single-energy images, which is illustrated by the exemplary measurements of the lumen diameter at monoenergetic extrapolations (90 keV, 2.4 cm for advanced monoenergetic algorithm (B) and 2.3 cm for standard monoenergetic images (E)) in comparison to the 90 kV single-energy acquisitions (H, 2.2 cm). The same window settings are used in A–I (bone window setting; center/width 300/1200 HU)

comparison with standard ME and SE data-sets [11–13], which is consistent with our results and accounts for the superior performance of the advanced ME reconstruction algorithm in the evaluation of in-stent lumen visibility.

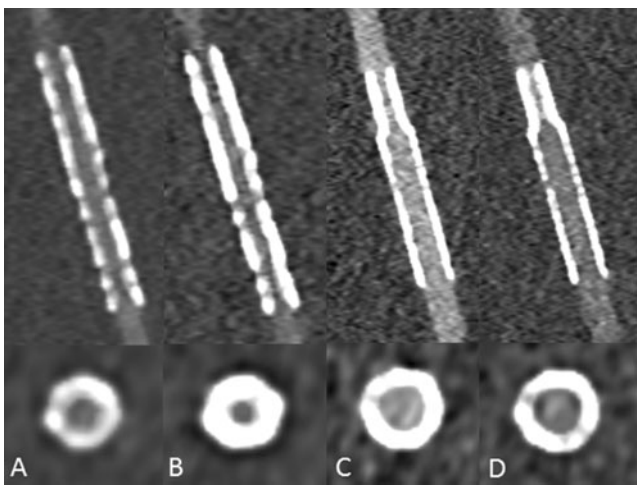

Fig. 5 Curved multiplanar reformats and cross section images of advanced monoenergetic reconstructions at 70 keV (A: 2.25 mm, C: 3.5 mm stent diameter) and of single-energy acquisition at 70 kV (B: 2.25, D: 3.5 mm stent diameter). The same window settings are used in A–F (bone window setting; centre/width 300/1200 HU). For the 2.25 mm stent diameter the lumen visualization is substantially decreased in advanced monoenergetic extrapolations (A) in comparison to the single-energy image (B) whereas the differences between the two acquisition modes are less pronounced for the 3.5 mm diameter stent (C and D). However, the increased contrast-to-noise ratio of the monoenergetic images is clearly perceptible

Iterative reconstruction algorithms contribute to improving the visualization of the stent struts and in-stent lumen, as shown using different algorithm generations [3, 5, 6, 21–23]. In our study, the application of ME reconstruction algorithms further improves the CNR and lumen visibility obtained with the iterative reconstruction algorithm, as demonstrated in comparison with the SE data-set.

Another important finding of our study is the effect of different keV levels on lumen visibility. The best result regarding lumen visibility and accuracy of measuring the true lumen diameter was observed with acquisitions at 130 keV, which is mainly attributable to the almost complete suppression of the

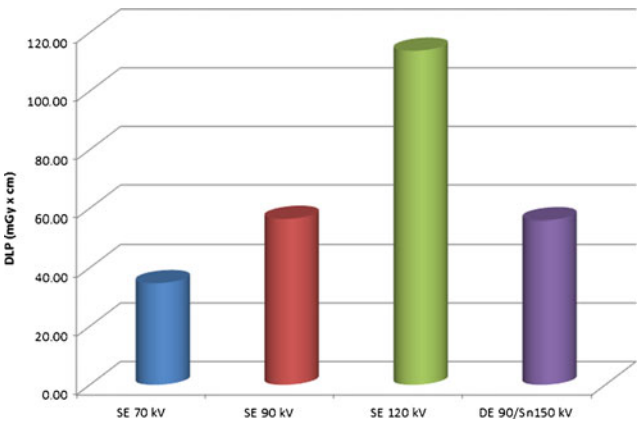

Fig. 6 Radiation dose comparison between single-energy and dual-energy prospective cardiac CT angiography. The slight difference in radiation dose observed among the three different stent diameters is due to a difference in the acquisition length. SE: single-energy; DE: dual-energy

blooming artefacts and the higher CNR observed at this energetic level. However, a significant drawback of the 130 keV dataset is that above 100 keV, the visibility of the stent itself is increasingly reduced, making measurements more challenging. Furthermore, it has to be taken into account that high keV levels might also lower the attenuation of calcified plaques. On the other hand, lowering the keV levelled to a progressive reduction in both CNR and lumen visualization, mainly due to increasing blooming artefacts secondary to increases in the attenuation of the metallic stent structure.

This result seems to be in consensus with a previous study performed with single-source DECT in a limited number of patients, where Stehli et al. demonstrated that the optimal visualization of the true in-stent lumen was achieved using the ME 140 keV data-set [14]. In our study, we decided to use an upper limit of 130 keV for the ME data-set given that stent structures were not assessable at all at higher energy levels. However, differences in scanner technology and reconstruction algorithms together with the significant variability in stent types and diameters observed in the clinical population represent substantial limitations for direct comparison of these two investigations.

To our knowledge, our study also represents the first direct comparison of SE acquisitions at low kV (70 and 90 kV) with the corresponding keV data.

As a result, we observed that ME data allow better visualization of stent structure and in-lumen visibility in comparison with SE acquisition due to a significant increase in CNR and decrease in associated blooming artefacts.

Finally, the radiation dose of the prospectively ECG-triggered DE acquisition was 49 % less than that of the prospectively ECG-triggered SE acquisition at 120 kV, and was comparable with the 90 kV SE scan. This remarkable result allows DECT imaging with a radiation dose comparable to low kV cardiac SE acquisitions, which could possibly expand the routine utilization of the technique.

Thus, the results of our study suggest that the current trend aimed at reducing kV at CCTA could perhaps not be the appropriate strategy for an optimal visualization of coronary stents. On the contrary, the utilization of high ME levels reconstructed from a DE acquisition could improve the in-stent visibility with a significant reduction in radiation dose compared with standard 120 kV acquisition.

The findings of this investigation should be analyzed in the light of its limitations. A major limitation is the phantom-based approach and further investigations in vivo are necessary to validate the clinical applicability of our results. Secondly, we did not increase keV levels beyond 130 keV, as visibility of stent struts and stent structure markedly decreased above 100 keV and the measurement of the lumen diameter became imprecise. Furthermore, we investigated only one stent type of each diameter and only strength 3 of the iterative reconstruction algorithm. It has been reported that stent lumen visibility varies significantly depending on the stent type, stent manufacturer, and stent material [24, 25], thus, our results are only valid for the tested drug-eluting stent systems in the investigated set-up. Furthermore, the calculation of lumen visualization values can be inaccurate, especially if the stent is not fully expanded, and stent parameters were measured manually, so both values may be influenced by a certain degree of error in measurements.

In conclusion, third-generation dual-source DECT with advanced monochromatic reconstructions substantially improves the in-lumen visibility of small stents in comparison with standard monoenergetic and single-energy CT data sets. In addition, with this approach, the use of high keV levels significantly improves lumen visualization by reducing blooming artefacts.

Acknowledgments The scientific guarantor of this publication is Carlo N. De Cecco. The authors of this manuscript declare relationships with the following companies: Dr. Schoepf is a consultant for and receives research support from Bayer, Bracco, GE, Medrad, and Siemens. Mr. Canstein is a Siemens employee. The authors state that this work has not received any funding. No complex statistical methods were necessary for this paper. Institutional Review Board approval was not required because the study was performed by using a thoracic phantom model. No study subjects or cohorts have been previously reported. Methodology: prospective, experimental, performed at one institution.

References

1. Mahnken AH (2012) CT imaging of coronary stents: past, present, and future. ISRN Cardiol 139823
2. Min JK, Swaminathan RV, Vass M, Gallagher S, Weinsaft JW (2009) High-definition multidetector computed tomography for evaluation of coronary artery stents: comparison to standard-definition 64-detector row computed tomography. J Cardiovasc Comput Tomogr 3:246–251
3. Gassenmaier T, Petri N, Allmendinger T et al (2014) Next generation coronary CT angiography: in vitro evaluation of 27 coronary stents. Eur Radiol 24:2953–2961
4. Ulrich A, Burg MC, Raupach R et al (2015) Coronary stent imaging with dual-source CT: assessment of lumen visibility using different convolution kernels and postprocessing filters. Acta Radiol 56:42–50
5. von Spiczak J, Morsbach F, Winklhofer S et al (2013) Coronary artery stent imaging with CT using an integrated electronics detector and iterative reconstructions: first in vitro experience. J Cardiovasc Comput Tomogr 7:215–222
6. Eisentopf J, Achenbach S, Ulzheimer S et al (2013) Low-dose dual-source CT angiography with iterative reconstruction for coronary artery stent evaluation. JACC Cardiovasc Imaging 6:458–465
7. Zhou Q, Jiang B, Dong F, Huang P, Liu H, Zhang M (2014) Computed tomography coronary stent imaging with iterative reconstruction: a trade-off study between medium kernel and sharp kernel. J Comput Assist Tomogr 38:604–612
8. Geyer LL, Glenn GR, De Cecco CN et al (2015) CT evaluation of small-diameter coronary artery stents: effect of an integrated circuit detector with iterative reconstruction. Radiology 276:706–714
9. Wichmann JL, Arbaciauskaite R, Kerl JM et al (2014) Evaluation of monoenergetic late iodine enhancement dual-energy computed

tomography for imaging of chronic myocardial infarction. Eur Radiol 24:1211–1218
10. Bamberg F, Dierks A, Nikolaou K, Reiser MF, Becker CR, Johnson TR (2011) Metal artifact reduction by dual energy computed tomography using monoenergetic extrapolation. Eur Radiol 21: 1424–1429
11. Bongers MN, Schabel C, Krauss B et al (2014) Noise-optimized virtual monoenergetic images and iodine maps for the detection of venous thrombosis in second-generation dual-energy CT (DECT): an ex vivo phantom study. Eur Radiol 25:1655–1664
12. Schabel C, Bongers M, Sedlmair M et al (2014) Assessment of the hepatic veins in poor contrast conditions using dual energy CT: evaluation of a novel monoenergetic extrapolation software algorithm. Röfo 186:591–597
13. Grant KL, Flohr TG, Krauss B, Sedlmair M, Thomas C, Schmidt B (2014) Assessment of an advanced image-based technique to calculate virtual monoenergetic computed tomographic images from a dual-energy examination to improve contrast-to-noise ratio in examinations using iodinated contrast media. Investig Radiol 49:586–592
14. Stehli J, Fuchs TA, Singer A et al (2014) First experience with single-source, dual-energy CCTA for monochromatic stent imaging. Eur Heart J Cardiovasc Imaging 16:507–512
15. Winklehner A, Goetti R, Baumueller S et al (2011) Automated attenuation-based tube potential selection for thoracoabdominal computed tomography angiography: improved dose effectiveness. Investig Radiol 46:767–773
16. Gilard M, Cornily JC, Pennec PY et al (2006) Assessment of coronary artery stents by 16 slice computed tomography. Heart 92:58–61
17. Carbone I, Francone M, Algeri E et al (2008) Non-invasive evaluation of coronary artery stent patency with retrospectively ECG-gated 64-slice CT angiography. Eur Radiol 18:234–243
18. Oncel D, Oncel G, Tastan A, Tamci B (2008) Evaluation of coronary stent patency and in-stent restenosis with dual-source CT coronary angiography without heart rate control. AJR Am J Roentgenol 191:56–63
19. Pugliese F, Weustink AC, Van Mieghem C et al (2008) Dual source coronary computed tomography angiography for detecting in-stent restenosis. Heart 94:848–854
20. Taylor AJ, Cerqueira M, Hodgson JM et al (2010) ACCF/SCCT/ACR/AHA/ASE/ASNC/NASCI/SCAI/SCMR 2010 appropriate Use criteria for cardiac computed tomography. A report of the AMERICAN college of Cardiology Foundation appropriate use criteria task force, the society of cardiovascular computed tomography, the American College of Radiology, the American Heart Association, the American Society of Echocardiography, the American Society of Nuclear Cardiology, the North American Society for Cardiovascular Imaging, the Society for Cardiovascular Angiography and Interventions, and the Society for Cardiovascular Magnetic Resonance. Circulation 122:e525–e555
21. Ebersberger U, Tricarico F, Schoepf UJ et al (2013) CT evaluation of coronary artery stents with iterative image reconstruction: improvements in image quality and potential for radiation dose reduction. Eur Radiol 23:125–132
22. Leipsic J, Heilbron BG, Hague C (2012) Iterative reconstruction for coronary CT angiography: finding its way. Int J Cardiovasc Imaging 28:613–620
23. Renker M, Geyer LL, Krazinski AW, Silverman JR, Ebersberger U, Schoepf UJ (2013) Iterative image reconstruction: a realistic dose-saving method in cardiac CT imaging? Expert Rev Cardiovasc Ther 11:403–409
24. Maintz D, Burg MC, Seifarth H et al (2009) Update on multidetector coronary CT angiography of coronary stents: in vitro evaluation of 29 different stent types with dual-source CT. Eur Radiol 19:42–49
25. Maintz D, Seifarth H, Raupach R et al (2006) 64-slice multidetector coronary CT angiography: in vitro evaluation of 68 different stents. Eur Radiol 16:818–826